Taylor & Francis
Taylor & Francis Group

Advanced Composite Materials

ISSN: (Print) (Online) Journal homepage: https://www.tandfonline.com/loi/tacm20

Delamination growth in curved composite beam at elevated temperatures

Young-Woo Truong, Viet-Hoai Hoang, Van-Tho Choe, Hyeon-Seok Nam & Jin-Hwe Kweon

To cite this article: Young-Woo Truong, Viet-Hoai Hoang, Van-Tho Choe, Hyeon-Seok Nam & Jin-Hwe Kweon (2021): Delamination growth in curved composite beam at elevated temperatures, Advanced Composite Materials, DOI: 10.1080/09243046.2021.1934952

To link to this article: https://doi.org/10.1080/09243046.2021.1934952

Advanced Composite Materials, 2021
https://doi.org/10.1080/09243046.2021.1934952

Delamination growth in curved composite beam at elevated temperatures

Young-Woo Truong [a,b], Viet-Hoai Hoang [a], Van-Tho Choe[a], Hyeon-Seok Nam [a] and Jin-Hwe Kweon[a]

[a]*School of Mechanical and Aerospace Engineering, Gyeongsang National University, Jinju, Korea;* [b]*Faculty of Mechanical Engineering, Le Qui Don Technical University, Hanoi, Vietnam*

(*Received 6 August 2020; accepted 23 May 2021*)

Delamination failure commonly appears in composite structures, especially those with curved regions, where a relatively high through-thickness stress is generally created. This study examined the delamination growth behavior of curved composite laminates at elevated temperatures. A four-point bending test was performed at room temperature, 100°C, and 125°C, where 125°C exceeds the epoxy glass transition temperature. We found that the failure load at 100°C was 32.5% lower than that at room temperature, whereas at 125°C, the failure load decreased by 64.5%. Additionally, the delamination growth process, that is, delamination propagation, varied significantly with temperature. Finite element analyses using cohesive elements were performed to determine reasonable sets of cohesive parameters that accurately represent the delamination behavior of the beam at high temperatures. The values of the cohesive parameters were identified considering the degradation owing to high temperature. A comparison of the numerical and experimental results revealed good agreement in terms of the failure load and modes. The effect of temperature on the failure mechanism was thoroughly discussed.

Keywords: composites; delamination; curved beam; elevated temperature; cohesive zone model

1. Introduction

Laminated composite materials are increasingly used in structural components in the aerospace, automotive, and marine industries owing to their high specific strength, high specific modulus, and low weight. One disadvantage of composite materials is that their interlaminar strength is relatively low compared with those in other directions because laminated composite materials are generally not through-thickness reinforced. Consequently, delamination failure, which is defined as separation of two adjacent laminae, is among the most common failures modes of composite structures [1].

Delamination in a composite component greatly decreases the stiffness and strength of the component and may cause catastrophic failure of the entire structure [2,3]. Delamination can originate from several sources, for example, curved/straight free edges, internal/external ply drops, corners/curvature, and skin–stiffener interaction [4].

Corresponding author. Young-Woo Nam Email: ywnam@gnu.ac.kr and Jin-Hwe Kweon Email: jhkweon@gnu.ac.kr

Composite structures with curved regions are widely used in the aerospace, automotive, and wind power industries, for example, in aircraft wings, spars, car frames, and wind turbine blades. Curvature-induced delamination is a serious concern in these applications; therefore, it has long been extensively investigated [5–10]. For example, Martin et al. [5] predicted the initiation and propagation of delamination in curved composite laminates. On the basis of finite element analysis and experiments, they reported the stress distribution in the undamaged curved laminate. Kress et al. [6] introduced a new mechanical model for calculating the through-thickness stress in singly curved laminates. The virtual crack closure technique (VCCT) and cohesive zone method are frequently used to simulate the delamination behavior of a composite structure. Wimmer et al. [7] examined delamination initiation and growth in an L-shaped laminated composite. In their study, delamination initiation was determined using the first-ply failure criterion, whereas the VCCT was applied to represent delamination propagation. The cohesive zone method is among the most powerful techniques for the simulation of delamination growth in curved composite laminates and has been used by numerous researchers [8–10]. Nguyen et al. [8] and Truong at al [9]. simulated delamination growth in curved laminated composite beams, and Gonoku et al. [10] numerically investigated the speed of delamination propagation. The authors [9,10] studied the delamination failure of curved composite beams under opening loads in directions perpendicular or parallel to one arm of the beams.

The four-point bending test described in ASTM 6415 is frequently adopted as an experimental method [8,11,12] to investigate the delamination behavior of curved composite laminates. Hao et al. [11] examined the effects of the curvature and thickness of a beam on delamination failure, and Nguyen et al. [8] considered the impact of fiber orientation. In another study, Ju et al. [12] reported the role of pin diameter and pin density in the delamination failure of curved composite beams through-thickness reinforced by z-pinning.

Most of these studies [5–12] focused on the delamination failure of composite structures at room temperature. The mechanical properties of a material generally deteriorate with increasing temperature, resulting in decreased stiffness, modulus, strength, and so on. Consequently, the performance of composite structures at high temperature must be examined.

Many studies have investigated the effects of high temperature on the structural behavior of composite laminates, such as the tensile, bending, and buckling behaviors. For instance, Li et al. [13] conducted tensile tests at temperatures of up to 250°C and described the effects of temperature on the stiffness, strength, and failure behavior of carbon/polyimide laminates. Sun and Yoon [14] characterized the effects of temperature on the inelastic and strength properties of AS4/PEEK composites by performing a simple tension test at various temperature. Mahieux et al. [15] conducted end-load bending experiments on a thermoplastic composite plate at elevated temperatures to characterize the failure modes. An experimental relationship between the flexural static and fatigue strengths and the temperature was plotted by Yasushi [16]. Lee et al. [17] and Srikanth et al. [18] investigated the buckling and post-buckling behaviors of laminated composite plates subjected to different temperature distributions. The effects of temperature on the static and fatigue behavior of composite laminates were also extensively studied by other researchers [19–23].

The degradation of the mechanical properties of composite materials with increasing temperature were also reported. Yoon and Kim [24] reported that the elastic moduli (E_2,

G_{12}) of carbon/epoxy laminates decreased linearly whereas E_1 and v_{12} did not change significantly as the temperature was increased to 140°C. Nguyen et al. [25] investigated the mechanical properties of a carbon-fiber-reinforced polymer (CFRP) based on the distinct microwave irradiation and found a lower elastic modulus and bending strength at higher temperature (or longer irradiation time). These studies [13–25] considered only a stable temperature range from room temperature to the glass transition temperature (T_g) of the matrix, where the mechanical properties of composite materials decrease linearly at higher temperatures. To simultaneously consider thermal and mechanical loading, the thermomechanical properties of graphite/epoxy were analytically derived by Chen at al [26]. according to the rule of mixture and the thermal resistance capacity of materials up to 3316°C. A continuous function describing the temperature-dependent material properties was also estimated by Zhang et al. [27] using an analytical model to examine the effects of coupled thermal and mechanical loading on the stress, displacement, and temperature distributions in a sandwich beam.

Fracture toughness, which is considerably affected by temperature, is another mechanical property that represents a material's resistance to crack propagation [28]. The fracture toughness and delamination behavior of composite materials at high temperature have also been studied [29–33]. Sjogren at al [29]. reported that the mode I fracture toughness at 100°C decreased slightly (by only 4%), whereas the mode II toughness was reduced by 30% compared with the values at 20°C. Similarly, Browning and Schwarts [30] reported a decrease of approximately 25% (from 149 to 112 J/m^2) in the mode I fracture toughness of the AS/3502 composite after postcuring at 177°C for 6 h. Coronado et al. [31] experimentally determined the mode I fracture toughness values of composite materials at six temperatures between −60°C and 90°C. They reported that the highest mode I fracture toughness was obtained at the highest temperature, 90°C; however, the lowest toughness was found not at the lowest temperature but at 0°C. Kim et al. [32] performed tensile tests at low, room, and high temperatures to investigate the effects of temperature on the transverse crack propagation and delamination growth behavior of a composite laminate. Street et al. [33] experimentally characterized the mode I and II fracture toughness of a graphite/epoxy composite as a function of overheating temperature up to 350°C.

According to a literature survey, the delamination behavior of composite structures with curved regions at high temperature has seldom been studied. Moreover, finite element analysis of delamination behavior using cohesive elements depends strongly on the choice of cohesive parameters [8,9,34,35]. However, there are no reports on how to choose a reasonable set of cohesive parameters to represent the delamination behavior of a composite structure at high temperatures. Therefore, in this study, we examined the initiation and propagation of delamination in curved composite laminates at elevated temperatures. Four-point bending tests of curved laminates at three temperatures ranging from room temperature to just above the glass transition temperature of the resin were performed. Finite element analyses using cohesive elements were performed to determine reasonable sets of cohesive parameters that accurately represent the delamination behavior of a beam at high temperatures. The values of the cohesive parameters were chosen considering the degradation owing to high temperature. A comparison of the numerical and experimental results revealed good agreement in terms of the failure load and modes. The effect of temperature on the failure mechanism is thoroughly discussed.

2. Experimental

2.1. *Curved composite beam*

A carbon/epoxy unidirectional prepreg (USN 200A, SK Chemicals Company, South Korea), was the main material used to fabricate a curved composite panel. Both sides of the laminates were additionally stacked on one layer of a carbon/epoxy fabric prepreg (WSN-3 KT) to avoid twisting of the panel during fabrication; the stacking sequence was $[45_F/(45/0/-45/90)_{3S}/45_F]$. A steel mold with an outer radius of 12 mm was designed and used to obtain a precise inner radius of the composite panel during the lay-up and curing stages in an autoclave [8,12]. In the curing cycle, specimens were cured under vacuum (approximately 0.95 ± 0.03 bar) without air compression for 3 h. The first cycle was performed at 80°C for 15 min, and the second cycle was performed at 120°C for 120 min. The temperature was increased from 25°C to 80°C in 30 min and from 80°C to 120°C in 20 min. The cured composite panels were then cut into several 25.4-mm-wide specimens by a diamond-disc cutting machine for the bending test. The curved specimens were 70 mm long and 25.4 mm wide, as shown in Figure 1. Figure 2 shows the composite beams fabricated for the bending test. Table 1 lists the mechanical properties of the USN and WSN-3 KT prepregs [36].

2.2. *Four-point bending test at elevated temperature*

The four-point bending test according to ASTM D6415 [37], which creates a pure bending region, was chosen in this study to examine the delamination growth process in the curved region of the beam (Figure 2). The test was performed using an Instron 5582 Universal Testing Machine (Illinois Tool Works Inc., Norwood, MA, USA) with a constant head speed of 0.5 mm/min. A high-quality camera was used to record the damage growth and failure modes of the specimens during the test.

To control the environmental temperature during testing, a chamber consisting of a heating system was used for the high-temperature bending test. The testing process at

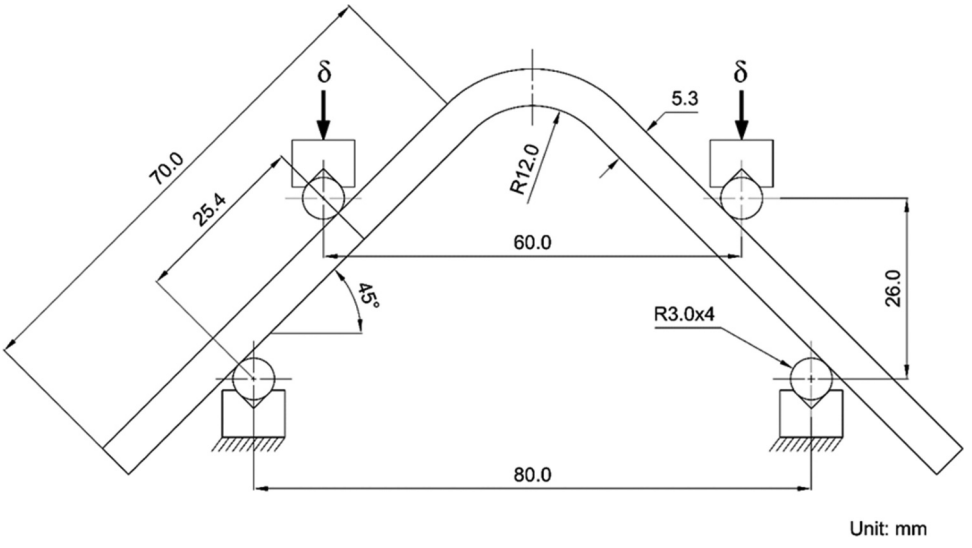

Figure 1. Specimen configuration and four-point bending test set-up.

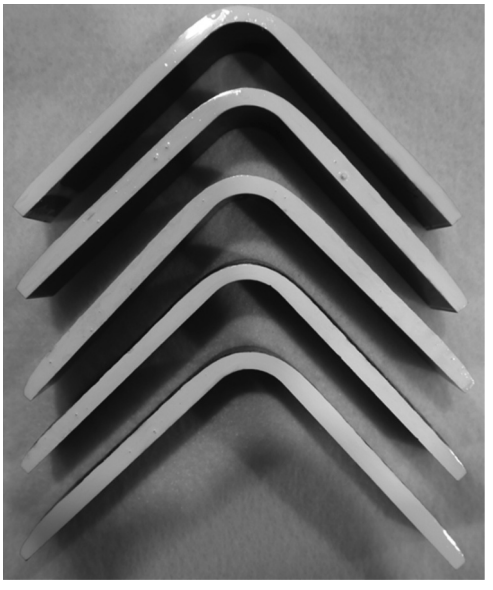

Figure 2. Manufactured curved composite beams.

Table 1. Mechanical properties of USN-200A and WSN-3K at room temperature [36].

Property	Symbol	USN-200A	WSN-3K
Elastic modulus (GPa)	E_1	125	56.4
	E_2	8.5	56.4
	E_3	8.5	9.6
Shear modulus (GPa)	G_{12}	3.2	3.6
	G_{13}	3.2	4.0
	G_{23}	3.2	4.0
Poisson's ratio	ν_{12}	0.3	0.062
	ν_{13}	0.3	0.20*
	ν_{23}	0.47	0.20*
Thickness (mm)	t	0.207	0.160

*: Assumed value.

high temperatures is illustrated in Figure 3. First, the curved specimen was carefully calibrated in the bending test setup. Second, the chamber was moved to the bending fixture until the entire fixture was within the chamber, and the door was closed. Third, the heating system was turned on for approximately 5 min to increase the temperature inside the chamber to the desired test temperature of 125°C. The chamber temperature was monitored using a thermal couple attached to the top surface of the specimen during the test. Finally, before the four-point bending test was performed, the specimen was held at the desired temperature for 3 min [38] to ensure a uniform temperature from the exterior to the interior.

As reported in our previous study [36], the mechanical performance of the same carbon-fiber-reinforced epoxy decreased only slightly when the ambient temperature was increased from room temperature to 100°C, but it decreased sharply at higher temperatures up to approximately the glass transition temperature. Therefore, we conducted the

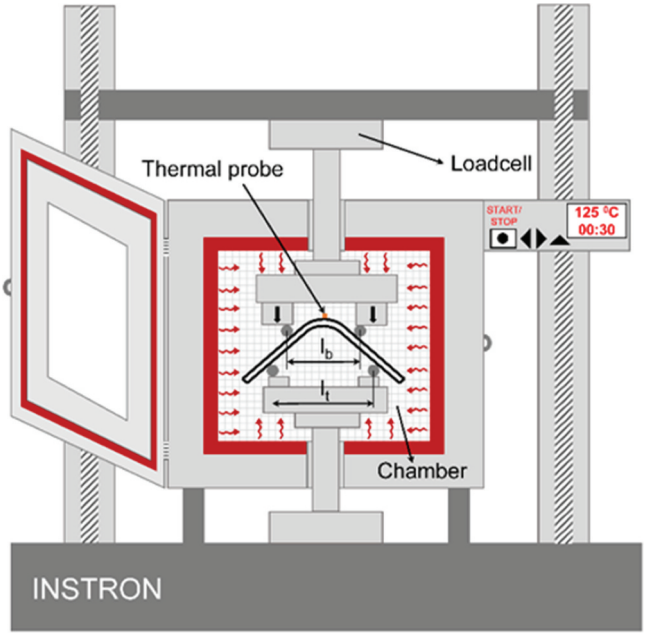

Figure 3. Schematic of bending test set-up at high temperature.

bending test in the same temperature range, but at only three temperatures (room temperature, 100°C, and 125°C) to save time.

3. Finite element analysis

Finite element analyses were performed using the commercial analysis software Abaqus.

3.1. *Finite element model*

Figure 4 presents the finite element model and boundary conditions for finite element analysis of the curved beam under a bending load. The incompatible mode eight-node brick element (C3D8I) and cohesive (COH3D8) elements were adopted to represent the behavior of composite laminae and the interfaces between two adjacent laminae, respectively. A stainless pin was modeled as a rigid body using four-node rigid elements (R3D4). A surface-to-surface contact available in the Abaqus software was chosen to represent the interaction between the pins and the curved laminates, where the contact properties were defined as in our previous studies [8,9]. Finite element analyses were performed to numerically investigate the delamination mechanism of the composite beams at high temperatures. The failure loads and modes predicted by the analyses were compared with the experimental data to evaluate the accuracy of the finite element models.

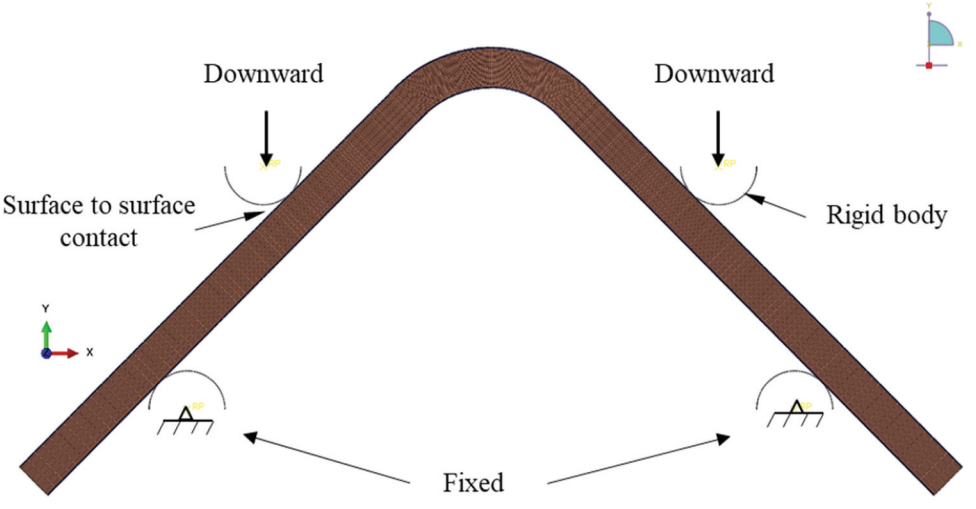

Figure 4. Finite element model and boundary conditions.

3.2. *Cohesive parameters*

The cohesive zone model is among the most powerful techniques for representing the debonding and delamination behavior of laminated composite structures. The behavior of cohesive elements is characterized by a traction–separation law based on the relationship between the three main parameters, the interface stiffness K^0, interface strength τ^0, and fracture toughness G_c. Figure 5 illustrates a bilinear traction–separation law that is frequently used [8,9,35,39–41] owing to its short analysis time and fast convergence. We adopted this bilinear law for all the cohesive elements implemented in the finite element model in this work.

Cohesive elements have been used to represent delamination between two adjacent laminae; the cohesive properties should be chosen according to the properties of the resin used. With increasing temperature, most of the mechanical properties of a material, such as strength and stiffness, are generally degraded. Therefore, the cohesive properties at the elevated temperatures (here, 100°C and 125°C) should be carefully chosen to accurately

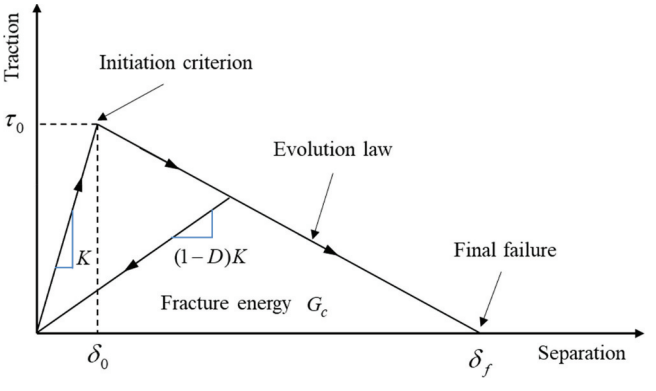

Figure 5. The bilinear traction-separation law.

represent the actual delamination behavior of the curved composite beams. The selection of the cohesive parameters is described in detail in section 4.2.

To represent the damage growth process, the mixed-mode response of the cohesive parameters should be determined. Waas et al. [42,43] presented an in-depth discussion of the commonly used traction–separation law in the simulation of crack initiation and growth. In [42], they proposed a new generalized formulation for mixed-mode crack propagation and demonstrated that mixed-mode fracture was accurately predicted by a comparison with the available experimental data. In this study, the Benzeggagh–Kenane (B–K) fracture criterion [44] was applied to represent the damage growth process. The B–K criterion is expressed as follows:

$$G^C = G_n^C + \left(G_s^C - G_n^C\right)\left(\frac{G_{st}}{G_T}\right)^{\eta} \tag{1}$$

where

$$G_{st} = G_s + G_t,$$

$$G_T = G_n + G_{st},$$

and η is a material parameter.

4. Results and discussion

4.1. *Experimental results*

4.1.1. *Failure loads and flexural properties*

$$CBS = \frac{M}{w} = \left(\frac{P}{2w\cos(\phi)}\right)\left(\frac{d_x}{\cos(\phi)} + (D+t)\tan(\phi)\right) \tag{2-1a}$$

$$d_x = \frac{l_b - l_t}{2} \tag{2-1b}$$

$$\sigma_r^{\max} = \frac{3M}{2wt\sqrt{r_i r_o}} \tag{2-2}$$

$$\sigma_r^{\max} = \frac{3.CBS}{2t\sqrt{r_i r_o}} \tag{2-3}$$

where

$P$is the load (kN),
$M$is the moment (kN·mm),
$CBS$is the curved beam strength (kN·mm/mm),
$w$is the specimen width (mm),
D is the diameter of the loading bar (mm),

$d_x$is the horizontal distance between the centerlines of two adjacent top and bottom rollers (mm),

$l_b$is the horizontal distance between the two bottom rollers (mm),

$l_t$is the horizontal distance between the two top rollers (mm),

$t$is the specimen thickness (mm),

$r_i$is the inner diameter of the specimen (mm),

$r_o$is the outer diameter of the specimen (mm),

and $\phi$is the angle of loading arm from the horizontal (degrees).

Figure 6 shows the load–displacement curves of the carbon fiber/epoxy prepreg at different temperatures under the four-point bending test. The failure load at the higher temperatures (100°C and 125°C) was much lower than that at 25°C. The average failure load from at least five specimens was calculated and is presented in detail in Figure 7. At 100°C and 125°C, the failure load decreased by 32.5% and 64.5%, respectively, compared to the value at 25°C.

Moreover, the curved beam strength (CBS) and maximum radial stress were estimated using Eq. (2–1a) [37] and Eq. (2–2) [45], respectively. Equation (2–2), which was derived by Kedward et al. [45], more accurately predicts the maximum radial stress for a wide range of geometries and accurate radial locations. Equation (2–3) represents the maximum radial stress, which was simplified to a linear relationship with the CBS by substituting Eq. (2–1a) into Eq. (2–2). As shown in Figure 7, the CBS and maximum radial stress were also lower at higher temperatures. At 100°C and 125°C, the CBS and maximum radial stress were 67.5% and 35.5%, respectively, of the values at 25°C; these decreases are similar to those of the failure load because of the proportional relationship between them in the above equations. For further comparison, the average CBS (774.69 N·mm/mm) and maximum radial stress (15.25 MPa) at 25°C can be considered. The ratio r_i/t is 2.26, and the average thickness t is 5.288 mm; the CBS and maximum

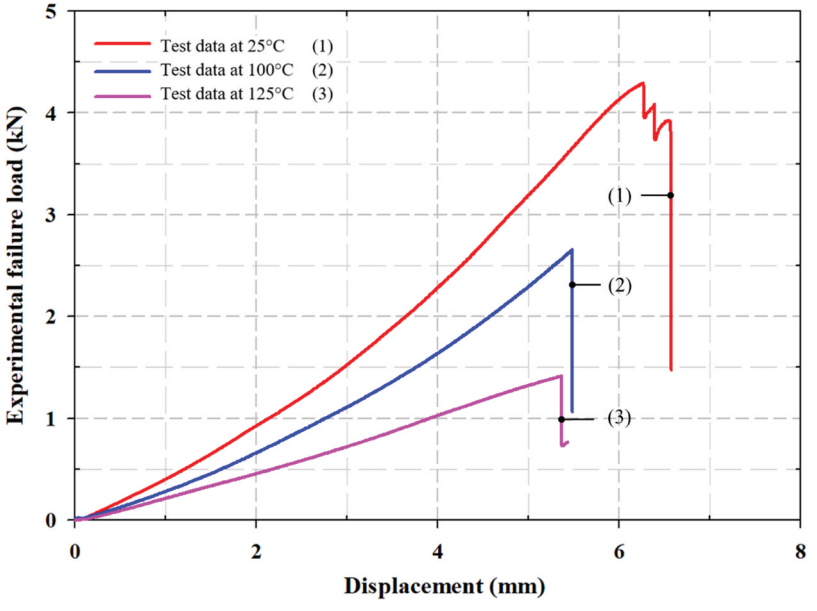

Figure 6. Representative load-displacement curves obtained from experiment.

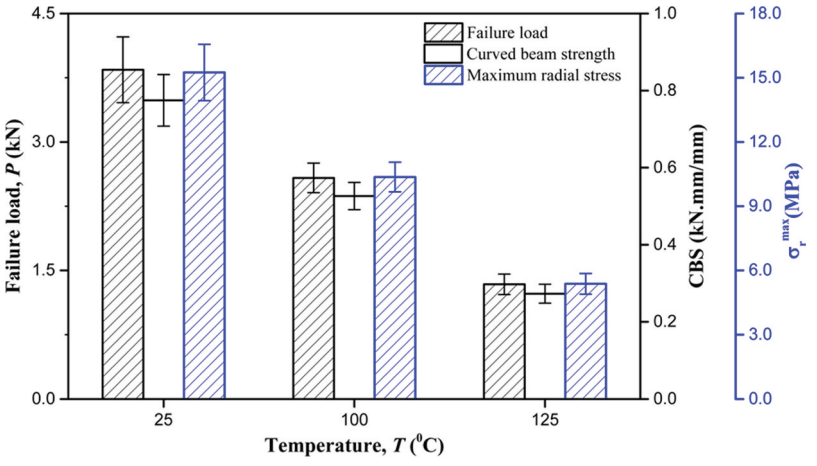

Figure 7. Average failure load and flexural properties of the beam at different temperatures.

radial stress can be approximately extrapolated from the work of Hao [11] as 500.0 N·mm/mm and 5.0 MPa, respectively. These differences in the CBS and maximum radial stress could arise from the material class, fiber volume fraction, and stacking sequence of the structure.

The effect of temperature on the CBS and maximum radial stress in this study is almost the same as the reported trend in the three-point bending strength of a 0° unidirectional CFRP [25] and flexural static strength of a satin-woven CFRP [16]. Therefore, this behavior is attributed to the softening of the matrix at high temperatures. Additionally, the flexural strength–temperature curve of previously reported composite structures [16,25] was apparently fitted by an exponential function. Thus, the flexural strength could be stable at lower temperatures and then decrease significantly near the glass transition temperature T_g, finally becoming saturated at higher temperatures. The glass transition temperature of the USN/epoxy composite in this research is 122°C [46]; thus, the serious degradation of the flexural properties was reasonable.

4.1.2. *Failure modes*

Figure 6 also illustrates the number of load drops at each test temperature during the four-point bending test. There are three load drops at 25°C and only one each at 100°C and 125°C. The number of drops were confirmed by the differences in the damaged area (Figure 8). At room temperature, the curved beam exhibited complicated failure with damage at various positions (Figure 8a). By contrast, interlaminar damage occurred at two locations (Figure 8b) and one location (Figure 8c) at 100°C and 125°C, respectively. Naturally, the first load drop can be attributed to the debonding of the matrix and the cracking of the fiber or matrix. However, at higher temperatures, the matrix cannot participate further in load transfer because it is softened. That is, the epoxy exhibits more ductile behavior at 100°C and 125°C, in contrast to the initial brittleness of the matrix at room temperature. Thus, the number of drops decreased.

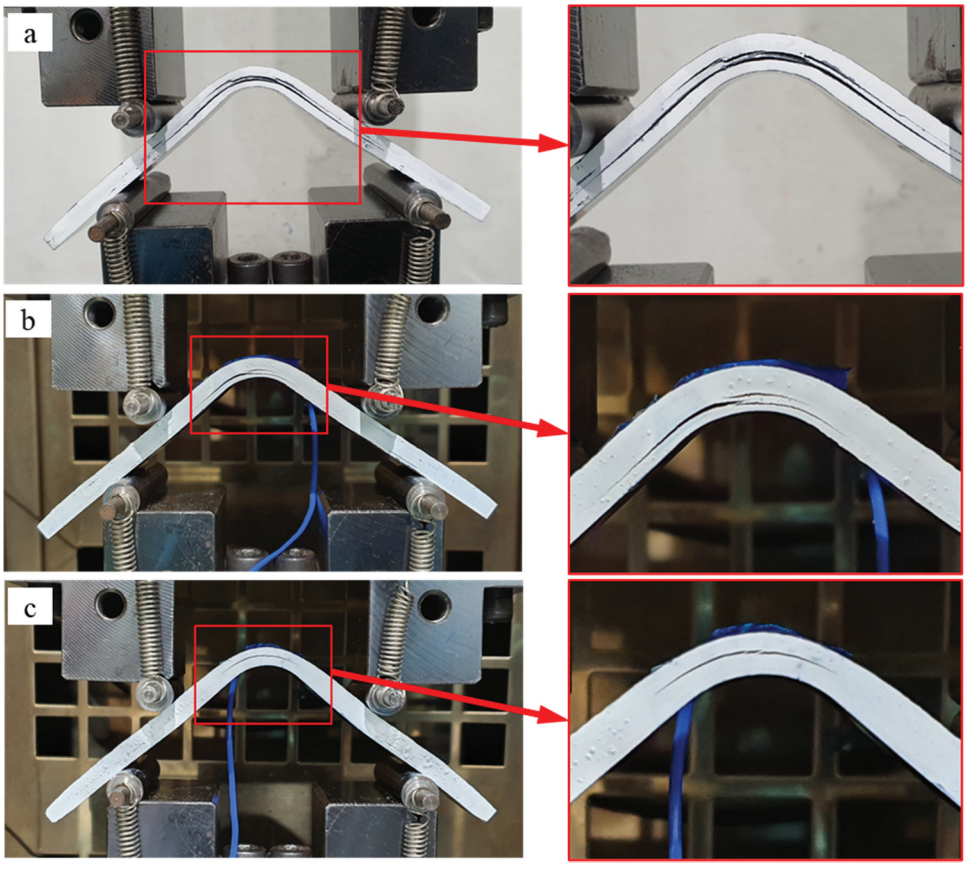

Figure 8. Failure modes at (a) room temperature, (b) 100°C, and (c) 125°C.

4.2. *Determination of cohesive parameter values at elevated temperatures*

A reasonable set of cohesive parameters that accurately represent the delamination behavior of a composite structure under loading is difficult to determine because it may depend on the materials used, structural configuration, and loading conditions [8–10,47]. We thus conducted a parametric study to examine the effects of the three main cohesive parameters (interface strength, interface stiffness, and fracture toughness) on the accuracy of the finite element analysis. The degradation of the composite mechanical properties resulting from high temperature was also considered in the analysis after the optimal cohesive parameters were determined.

4.2.1. *Interface strengths*

As reported in an investigation of the delamination failure of composite beams under opening loads [8,9], the predicted failure load depended strongly on the chosen values of the cohesive interface strengths. Therefore, we first considered only the effect of interface strength, where the normal interface strength ranged from 10 to 50 MPa, and the two shear strengths were calculated from the normal value [9,39] to examine the load–displacement responses of the beam at different temperatures. The other cohesive

Table 2. Cohesive parameters.

Initial stiffness	Interfacial strength		Fracture toughness	
K_n^0, K_s^0, K_t^0 (N/mm^3)	τ_n^0 (MPa)	$\tau_s^0 = \tau_t^0$ (MPa)	G_{Ic} (N/mm)	$G_{IIc} = G_{IIIc}$ (N/mm)
1.0×10^6	10	16	0.28	0.82
	20	32		
	30	48		
	40	64		
	50	80		

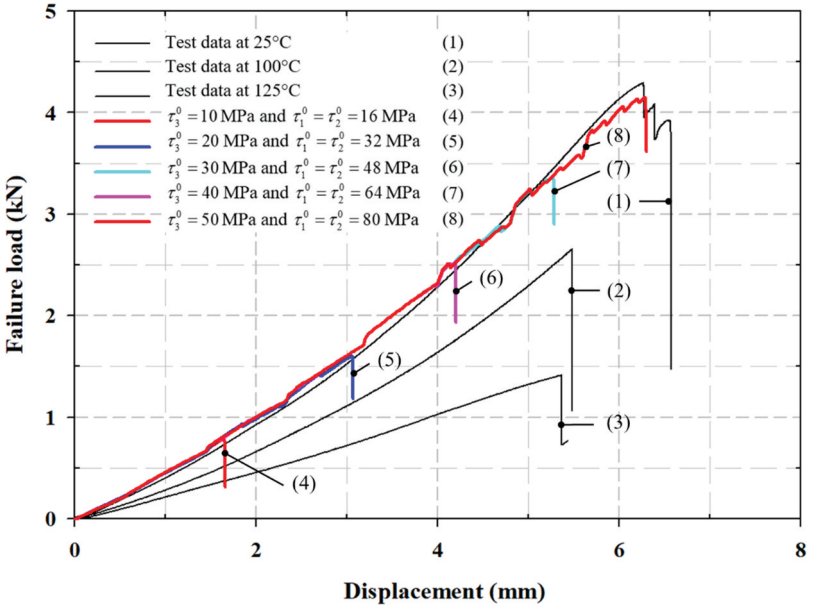

Figure 9. Effect of interface strength on the prediction of failure loads.

parameters, interface stiffness and fracture toughness, were fixed and are listed in Table 2. The load–displacement responses were obtained as shown in Figure 9. Only the response of the beam at room temperature was well-predicted using interface strengths of 50 and 80 MPa, where the predicted failure load was 4.15 kN, with an error of only 8.0% compared to the experimental data. These interface strengths are both lower than those selected by Nguyen et al. [8] ($\tau_3^0 = 58$ MPa and $\tau_1^0 = \tau_2^0 = 90.5$ MPa), where those authors also examined the delamination failure of a curved composite beam under a four-point bending load. The difference may be due to the differences in the through-thickness strengths of the composite materials used and the beam configurations.

At the selected interface strengths, ($\tau_3^0 = 30$ MPa, $\tau_1^0 = \tau_2^0 = 48$ MPa) and ($\tau_3^0 = 20$MPa, $\tau_1^0 = \tau_2^0 = 32$MPa), the predicted failure loads were 2.50 and 1.65 kN, which are closest to the experimental failure load at 100°C and 125°C, with prediction errors of −5.7% and +25%, respectively. The use of interface strengths of $\tau_3^0 = 13$ MPa and $\tau_1^0 = \tau_2^0 = 19.5$ MPa resulted in a predicted failure load of 1.31 kN, with an error of

−4%. Additionally, the corresponding displacements at beam failure obtained from the finite element analyses differed significantly from those observed in experimentally. These large prediction errors of both the failure load and displacement at failure show that the delamination response of the beams at 100°C and 125°C was poorly predicted.

We can conclude from these inaccurate prediction results that not only the interface strengths but also the other cohesive parameters may contribute to the representation of the delamination behavior of the beam at elevated temperatures. Therefore, we additionally conducted a parametric study on the effects of interface stiffness and fracture toughness on the numerical results to identify reasonable sets of cohesive parameters that accurately represent the delamination response of the beam at high temperatures.

4.2.2. *Interface stiffness*

According to the literature, values between 1×10^3 and 1×10^7 N/mm^3 are frequently adopted for the stiffness of the cohesive element (interface stiffness) to efficiently describe the delamination behavior of composite structures [8,9,35,48,49]. As shown in Figure 9, the chosen stiffness of 1×10^6 N/mm^3 yielded a load–displacement curve that matched the experimental curve well at room temperature. At the high temperatures (100°C and 125°C), the cohesive stiffness is degraded; therefore, values lower than those at room temperature should be selected. Six values of the interface stiffness between 1×10^2 and 1×10^5 N/mm^3 were adopted to examine the impact of stiffness on failure load prediction at the high temperatures. The normal and shear interface strengths were fixed at $\tau_3^0 = 13$ MPa and $\tau_1^0 = \tau_2^0 = 19.5$ MPa, whereas the fracture toughness values were chosen to be similar to those in Table 2. The load–displacement curves were obtained (Figure 10). The slope of the obtained load–displacement curve decreased as the cohesive stiffness decreased. However, the relationship between the slope and the

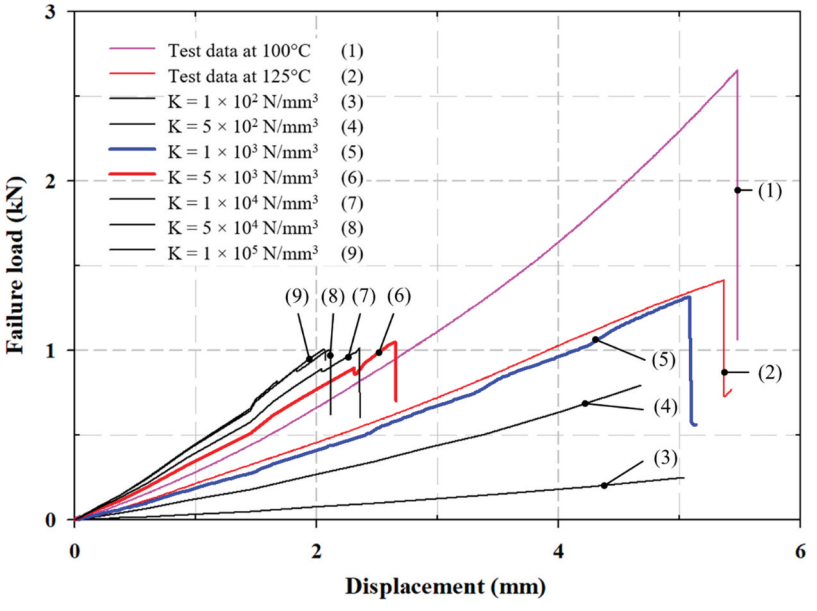

Figure 10. Effect of interface stiffness on the prediction of failure loads.

cohesive stiffness was not linear. Specifically, the slope of the curve varied slightly as the cohesive stiffnesses varied between 1×10^5 and 1×10^4 N/mm^3, whereas the slope decreased considerably as the stiffness decreased from 5×10^3 to 1×10^2 N/mm^3. Among the considered stiffness values, 5×10^3 and 1×10^3 N/mm^3 yielded the best numerical load–displacement responses of the beam at 100°C and 125°C, respectively. The strong effect of the interface stiffness on the slope of the predicted load–displacement curve found in this study is very different from that reported in Refs. [8,9], where the authors considered a small range of interface stiffness, from 26×10^3 to 1×10^8 N/mm^3.

Because the chosen set of cohesive parameters ($\tau_3^0 = 20$ MPa and $\tau_1^0 = \tau_2^0 = 32$ MPa, $K_n^0 = K_s^0 = K_t^0 = 1 \times 10^3$ N/mm^3) resulted in poor failure prediction of the beam at 125°C, a numerical method was employed to determine effective values of the interface strength to improve the prediction. It was found that using strengths of $\tau_3^0 = 13$ MPa and $\tau_1^0 = \tau_2^0 = 19.5$ MPa resulted in a predicted failure load of 1.31 kN, with a prediction error of only 4%. At 100°C, the use of cohesive parameters of $\tau_3^0 = 30$ MPa and $\tau_1^0 = \tau_2^0 = 48$ MPa, $K_n^0 = K_s^0 = K_t^0 = 5 \times 10^3$ N/mm^3 yielded a failure load of 2.81 kN, with an error of 5.2%. Finally, sets of cohesive parameters for accurate simulation of the delamination failure of the beams at high temperatures were chosen and are listed in Table 3. The interface stiffness does not affect the predicted failure load but does significantly affect the corresponding displacement. For instance, the obtained displacement increases by approximately 2.5 times as the stiffness is decreased from 1×10^5 to 1×10^3 N/mm^3.

4.2.3. *Fracture toughness*

At room temperature, the mode I and mode II fracture toughness of the USN-200 composite laminate were experimentally observed to be 0.28 and 0.82 N·mm [8,9], respectively. Here, the impact of the decrease in fracture toughness on the behavior of the beam at 125°C was considered by performing finite element analyses using two assumed values of the fracture toughness, which were 75% and 50% of the mode I and mode II fracture toughness at room temperature, respectively. The selected values of the other cohesive parameters were similar to those in Table 3. The predicted failure loads exhibited a maximum difference of only 0.5% between the three sets of fracture toughness values (Figure 11). The slopes of the load–displacement curves did not differ significantly. These minor differences indicate that the degradation of the fracture toughness resulting from increased temperature has no effect on the predicted load or delamination mechanism.

4.3. *Degradation of composite material properties at high temperatures*

Many efforts have been made to estimate the degradation of the mechanical properties of composite materials at elevated temperature [24–27]. As reported by Chen et al. [26], at a temperature of 200°C, which is close to the glass transition temperature of the resin used, the Young's modulus in the fiber direction did not decrease, whereas those in the other directions were reduced by approximately 20%, from 13.1 to 10.3 GPa. Choi et al. [36] conducted tensile tests on multi-angle and 90° laminates made from the same composite material at 100°C and 125°C. They reported reductions in tensile strength of only 1% and 7.7% at 100°C for the multi-angle and 90° laminates, respectively,

Table 3. Chosen cohesive parameters at different temperatures.

	Initial stiffness	Interfacial strength		Fracture toughness	
Cohesive zone model ID	K_n^0, K_s^0, K_t^0 (N/mm^3)	τ_n^0 (MPa)	$\tau_s^0 = \tau_t^0$ (MPa)	G_{Ic} (N/mm)	$G_{IIc} = G_{IIIc}$ (N/mm)
Room temperature	1.0×10^6	58	80	0.28	0.82
100°C	5.0×10^3	30	48		
125°C	1.0×10^3	13	19.5		

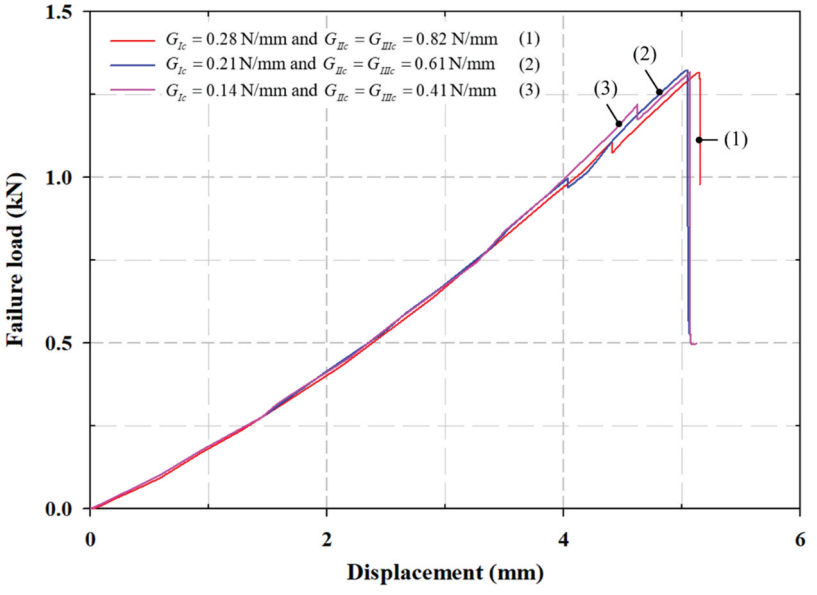

Figure 11. Effect of fracture toughness degradation at 125°C.

compared to those at room temperature; however, at 125°C, the reductions were 20.6% and 60.4%, respectively. We thus considered the degradation of the composite material only in the bending test at 125°C. We used Chen's method to roughly estimate the mechanical properties of the USN-200 composite laminate at 125°C to consider the effects of the degradation of composite materials on the analysis results. Specifically, at 125°C, the mechanical properties of the USN material that were not related to fiber direction (E_2, E_3, G_{12}, G_{13}, and G_{23}) were degraded and were simply estimated to be 70%, 60%, or 50% of the values at room temperature. Similarly, the properties of the WSN material at 125°C were also determined. Figure 12 shows the load–displacement responses of the beam at 125°C considering the decrease in mechanical properties caused by the high temperatures. The four predicted load–displacement curves showed only slight differences in the displacement at failure. Specifically, the four predicted failure loads are the same, whereas the maximum deviation in the displacement is only 7.6%.

The slight differences confirmed that the degradation of the composite material at the high temperatures had a negligible effect on the analysis results. The reason is that in the finite element analyses, we already considered the degradation of the mechanical properties of the composite material at the high temperatures by decreasing the cohesive parameters, that is, the strength and stiffness values (see Table 3). Therefore, additional consideration of the material property degradation of the composite material itself was unnecessary.

4.4. *Prediction of failure mode*

A high through-thickness stress in the curved region results in the delamination failure of a curved composite beam. In these finite element models using cohesive elements, the through-thickness stresses must be lower than the chosen critical normal interface strength. Figure 13 shows the distribution of the through-thickness stress of the beams

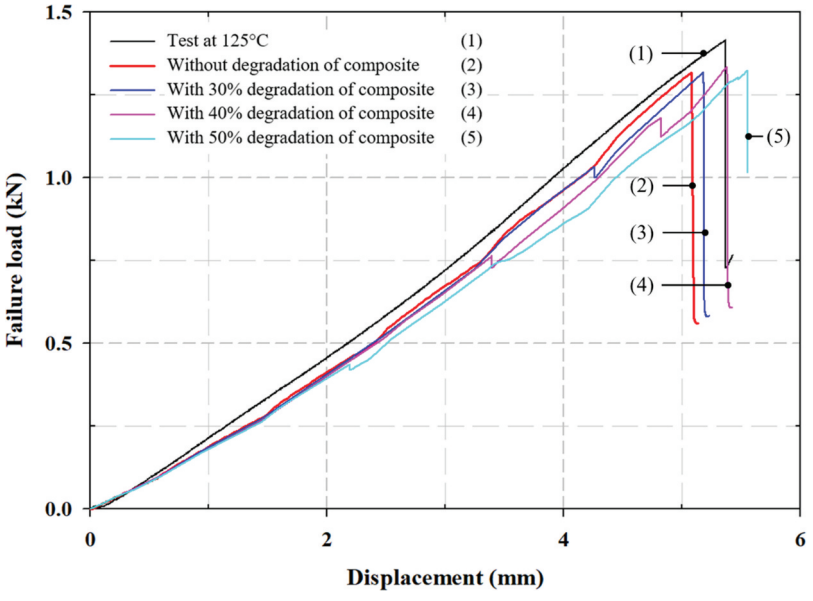

Figure 12. Effect of composite material degradation at high temperatures.

at (a) room temperature, (b) 100°C, and (c) 125°C, where the applied load reached approximately 95% of the predicted failure load before delamination initiation, confirming good agreement between the maximum stress and the corresponding critical strength of 50, 30, and 13 MPa, respectively.

The experimentally observed and simulated deformation and delamination failures of the beam at different temperatures are illustrated in Figure 14. The test data (left side) and numerical results (right side) are in good agreement. Additionally, the predicted failure modes are in good agreement with the test data for the length of delamination, which is shortest at 125°C and longest at room temperature.

This result is consistent with the test data, where the higher temperatures resulted in a lower failure load and less displacement of the beam (see section 4.1.1). In addition, asymmetric cracks along the specimen were found in both the numerical and experimental results, which are similar to those reported by Nguyen et al. [8]. These cracks could be attributed to the appearance of ±45° laminates that are not in-plane symmetric [8]. In particular, catastrophic delamination was found only at room temperature, whereas the failures were less serious at high temperature.

5. Conclusions

The delamination failure of a curved composite beam at elevated temperatures was experimentally and numerically investigated. Four-point bending tests were performed at three temperatures; the results showed that the failure loads at 100°C and 125°C were 32.5% and 64.5% lower than those at room temperature, respectively. Finite element analyses using cohesive elements were performed to identify reasonable sets of cohesive parameters that accurately represent the delamination behavior of the beam at high temperatures. The experimental load–displacement curve could be efficiently fitted considering the effects of interface stiffness, interface strength, and fracture toughness

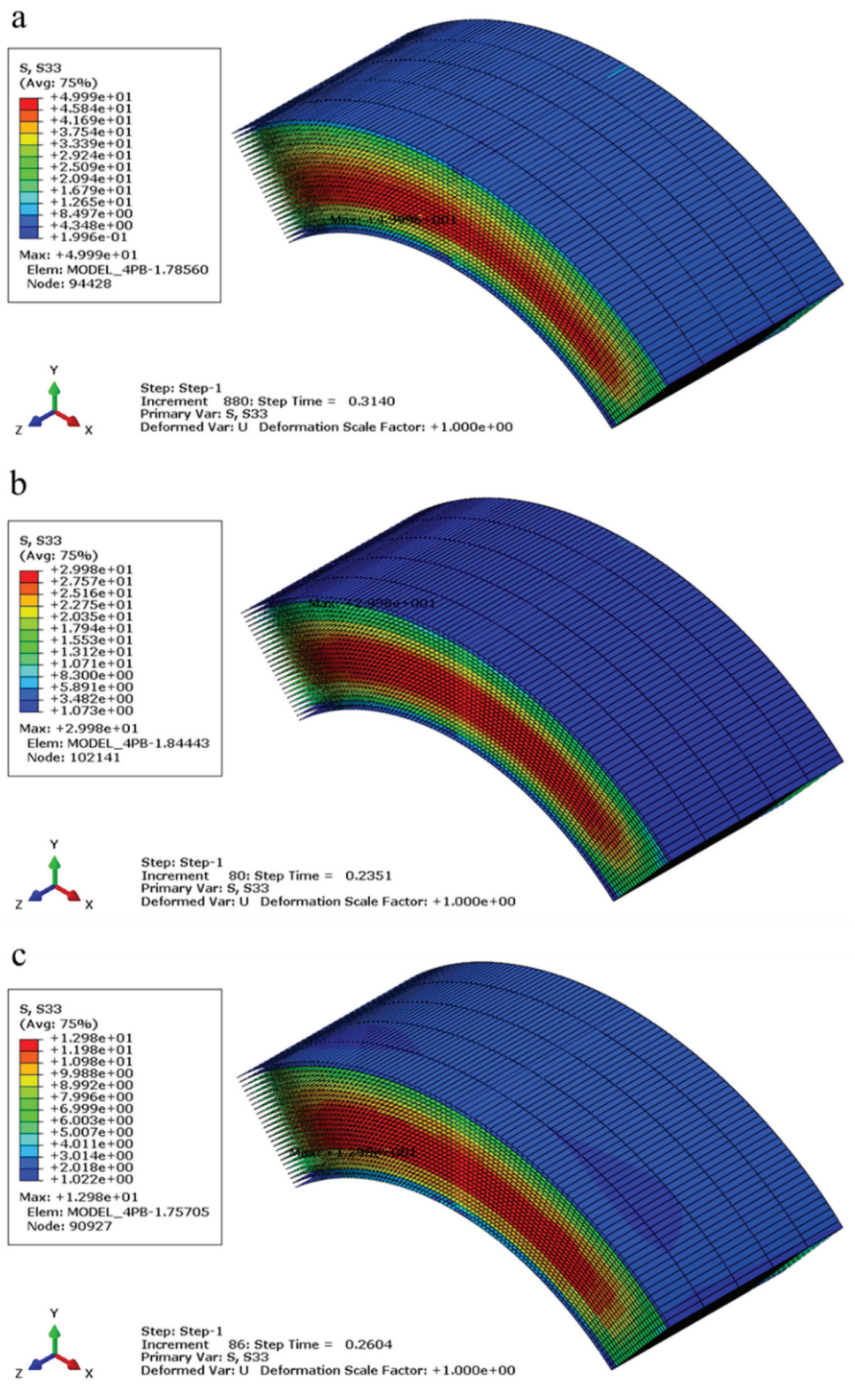

Figure 13. Distributions of through-thickness stresses of cohesive elements at (a) room temperature, (b) 100°C, and (c) 125°C.

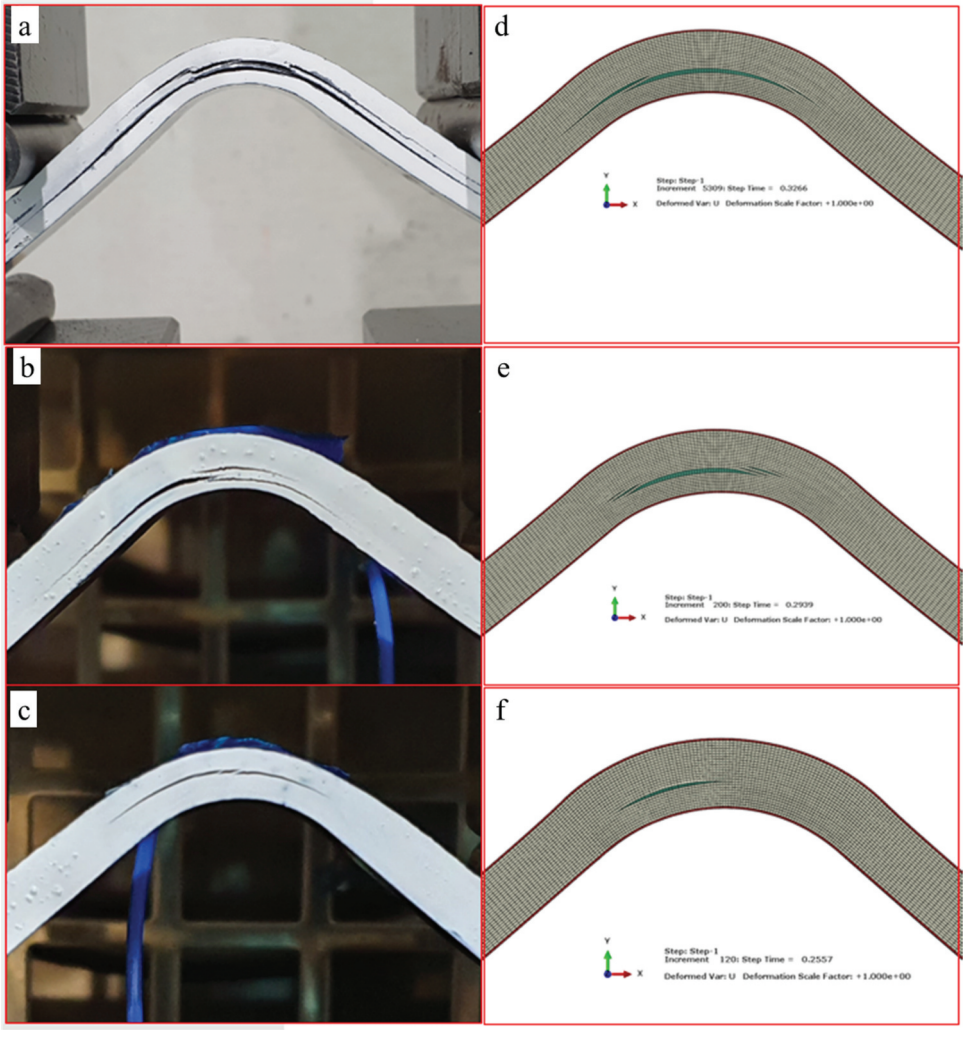

Figure 14. Deformed shapes of the beam at (a,d) room temperature, (b,e) 100°C, and (c,f) 125°C.

on the predicted displacement, failure load, and slope of the load–displacement curve, respectively. Three sets of parameters that best described the delamination behavior of the beams at the examined temperatures were obtained. A comparison of the numerical and experimental results revealed good agreement in the failure load and modes, with a maximum prediction error of 7.6%. The effect of temperature on the failure mechanism was also discussed.

Acknowledgements

This work was supported by the National Research Foundation of Korea (NRF) Grant funded by the Ministry of Science and ICT (NRF-2017R1A5A1015311).

Disclosure of potential conflicts of interest

No potential conflict of interest was reported by the authors.

ORCID

Young-Woo Truong http://orcid.org/0000-0003-2108-9043
Viet-Hoai Hoang http://orcid.org/0000-0002-6168-3402
Hyeon-Seok Nam http://orcid.org/0000-0001-9249-2169

References

[1] Bucinell RB. Composite materials: fatigue and fracture (7th volume). Philadelphia, PA: American Society for Testing and Materials (ASTM); 1998.
[2] Patel N, Rohatgi V, Lee JL. Micro scale flow behavior and void formation mechanism during impregnation through a unidirectional stitched fiberglass mat. Polym Eng Sci. 1995;35 (10):837–851.
[3] Rohatgi V, Patel N, Lee JL. Experimental investigation of flow induced microvoids during impregnation of unidirectional stitched fiberglass mat. Polym Composites. 1996;17 (2):161–170.
[4] Sridharan S. Delamination behaviour of composites. s: CRC Press LLC, 2008.
[5] Martin RH, Jackson WC Damage prediction in cross-plied curved composite laminates. NASA Technical Memorandum 104089, USAAVSCOM Technical Report 91-B-009; 1991.
[6] Kress G, Roos R, Barbezat M, et al. Model for interlaminar normal stress in singly curved laminates. Compos Struct. 2005;69(4):458–469.
[7] Wimmer G, Schuecker C, Pettermann HE. Numerical simulation of delamination in laminated composite components – a combination of a strength criterion and fracture mechanics. Compos Part B. 2009;40(2):158–165.
[8] Nguyen KH, Ju HW, Truong VH, et al. Delamination analysis of multi-angle composite curved beams using an out-of-autoclave materials. Compos Struct. 2018;183:320–330.
[9] Truong VH, Nguyen KH, Park SS, et al. Failure load analysis of C-shaped composite beams using a cohesive zone model. Compos Struct. 2018;184:581–590.
[10] Gözlüklü B, Coker D. Modeling of the dynamic delamination ofL-shaped unidirectional laminated composites. Compos Struct. 2012;94(4):1430–1442.
[11] Hao W, Ge D, Ma Y, et al. Experimental investigation on deformation and strength of carbon/ epoxy laminated curved beams. Polym Test. 2012;31(4):520–526.
[12] Ju HW, Nguyen KH, Chae SS, et al. Delamination strength of composite curved beams reinforced by grooved stainless-steel Z-pins. Compos Struct. 2018;180:497–506.
[13] Li L, Jia P, Pan W. Temperature effect on the tensile behaviors of carbon/polyimide composite laminate. Proc IMechE, Part C: J Mechanical Engineering Science. 2016;231(24):4592–4602.
[14] Sun CT, Yoon KJ. Characterization of elastic–plastic behavior of AS-4/PEEK thermoplastic composite for temperature variation. J Composite Mater. 1991;25(10):1297–1313.
[15] Mahieux C, Russell BE, Reifsnider KL. Stress rupture of unidirectional high performance thermoplastic composites in end-loaded bending at elevated temperatures, Part I: experimental characterization of the failure mode. J Composite Mater. 1998;32(14):1311–1321.
[16] Miyano Y, McMurray MK, Enyama J, et al. Loading rate and temperature dependence on flexural fatigue behavior of a satin woven CFRP laminate. J Compos Mater. 1994;28 (13):1250–1260.
[17] Lee JJ, Oh IK, Lee I, et al. Thermal post-buckling behavior of patched laminated panels under uniform and non-uniform temperature distributions. Compos Struct. 2002;55(2):137–145.
[18] Srikanth G, Kumar A. Post buckling response and failure of symmetric laminates under uniform temperature rise. Compos Struct. 2003;59(1):109–118.
[19] Chen LW, Chen LY. Thermal postbuckling analysis of laminated composite plates by the finite element method. Compos Struct. 1989;12(4):257–270.
[20] Chen LW, Chen LY. Thermal postbuckling behaviors of laminated composite plates with temperature-dependent properties. Compos Struct. 1991;19(3):267–283.

[21] Argyris J, Tenek L. Postbuckling of composite laminates under compressive loads and temperature. Comp Meth Appl Mech Eng. 1995;128(1–2):49–80.
[22] Jen MHR, Tseng YC, Kung H-K, et al. Fatigue response of APC-2 composite laminates at elevated temperatures. Compos Part B. 2008;39(7–8):1142–1146.
[23] Brillhart M, Botsis J. Fatigue fracture behavior of PEEK: 2. Effects of thickness and temperature. Polymer. 1992;33(24):5225–5232.
[24] Yoon KJ, Kim JS. Prediction of thermal expansion properties of carbon/epoxy laminates for temperature variation. J Compos Mater. 2000;34(2):90–100.
[25] Nguyen PN, Kubouchi M, Sakai T, et al. Relationship of mechanical properties and temperature of carbon fiber-reinforced plastics under microwave irradiation. Clean Technol Envir. 2012;14(5):943–951.
[26] Chen JK, Sun CT, Chang CI. Failure analysis of a graphite/epoxy laminate subjected to combined thermal and mechanical loading. J Compos Mater. 1985;19(5):408–423.
[27] Zhang Z, Zhou D, Fang H, et al. Analysis of laminated beams with temperature-dependent material properties subjected to thermal and mechanical loads. Compos Struct. 2019;227:111304.
[28] Wang QZ, Jia XM, Kou SQ, et al. More accurate stress intensity factor derived by finite element analysis for the ISRM suggested rock fracture toughness specimen-CCNBD. Int J Rock Mech Min Sci. 2003;40(2):233–241.
[29] Sjogren A, Asp LE. Effects of temperature on delamination growth in a carbon/epoxy composite under fatigue loading. Int J Fatigue. 2002;24(2–4):179–184.
[30] Browning CE, Schwartz HS, Delamination resistant composite concepts, in Composite Materials Testing and Design 7th Conference, ed. Whitney JE, STP 893, ASTM Philadelphia, 1986, 256–265.
[31] Coronado P, Argüelles A, Viña J, et al. Influence of temperature on a carbon-fibre epoxy composite subjected to static and fatigue loading under mode-I delamination. Int J Solids Struct. 2012;49(21):2934–2940. .
[32] Kim HS, Wang WX, Takao Y. Evaluation by FEM of temperature-dependent damage behavior in quasi-isotropic carbon/epoxy laminates. Adv Compos Mater. 1999;8(3):247–257.
[33] Street KN, Russell AJ, Bonsang F. Thermal damage effects on delamination toughness of a graphit/epoxy composite. Compos Sci Technol. 1988;32(1):1–14.
[34] Saeedifar M, Fotouhi M, Ahmadi Najafabadi M, et al. Prediction of delamination growth in laminated composites using acoustic emission and cohesive zone modeling techniques. Compos Struct. 2015;94(5):1483–1494.
[35] Turon A, Davila CG, Camanho PP, et al. An engineering solution for mesh size effects in the simulation of delamination using cohesive zone models. Eng Fract Mech. 2007;74 (10):1665–1682.
[36] Choi HS, Kwak BS, Park SM, et al. Tensile strength of composite bonded scarf joint in various thermal environmental conditions. Adv Compos Mater. 2020. DOI:10.1080/09243046.2019.1710679
[37] Standard test method for measuring the curved beam strength of a fiber-reinforced polymer-matrix composite. ASTM Standard D6415/D6415M.
[38] AGATE WP3.3-033051-134. Advanced general aviation transport experiments. Wichita: National Institute for Aviation Research Wichita State University Wichita; 2002.
[39] Turon A, Camanho PP, Costa J, et al. Accurate simulation of delamination growth under mixed-mode loading using cohesive elements: definition of interlaminar strengths and elastic stiffness. Compos Struct. 2010;92(8):1857–1864.
[40] Zhao L, Gong Y, Zhang J, et al. Simulation of delamination growth in multidirectional laminates under mode I and mixed mode I/II loadings using cohesive elements. Compos Struct. 2014;116(1):509–522.
[41] Truong VH, Kwak BS, Roy R, et al. Cohesive zone method for failure analysis of scarf patch-repaired composite laminates under bending load. Compos Struct. 2019;222:110895.
[42] Nguyen N, Waas AM. A novel mixed-mode cohesive formulation for crack growth analysis. Compos Struct. 2015;156:253–262.
[43] Joseph AP, Davidson P, Waas AM. Open hole and filled hole progressive damage and failure analysis of composite laminates with a countersunk hole. Compos Struct. 2018;203:523–538.

[44] Benzeggagh ML, Kenane M. Measurement of mixed-mode delamination fracture toughness of unidirectional glass/epoxy composites with mixed-mode bending apparatus. Compos Sci Technol. 1996;56(4):439–449.
[45] Kedward KT, Wilson RS, McLean SK. Flexure of simply curved composite shapes. Composites. 1989;20(6):527–536.
[46] https://www.skchemicals.com/page/business/bs_skyflex.do
[47] Geleta TN, Woo K, Lee B. Delamination behavior of L-shaped laminated composites. Int J Aeronaut Space Sci. 2018;19(2):363–374.
[48] Zou Z, Reid SR, Li S, et al. Modelling interlaminar and intralaminar damage in filament-wound pipes under quasi-static indentation. J Compos Mater. 2002;36(4):477–499.
[49] Camanho PP, Davila CG, De Moura MF. Numerical simulation of mixed-mode progressive delamination in composite materials. J Compos Mater. 2003;37(16):1415–1438.